RSC Advances

PAPER

View Article Online
View Journal | View Issue

Cite this: *RSC Adv.*, 2023, **13**, 29512

Influence of core size on self-assembled molecular networks composed of C_{3h}-symmetric building blocks through hydrogen bonding interactions: structural features and chirality†

Matsuhiro Maeda,[a] Kotoka Oda,[a] Ichiro Hisaki [b] and Kazukuni Tahara *[a]

Received 23rd August 2023
Accepted 26th September 2023

DOI: 10.1039/d3ra05762c

rsc.li/rsc-advances

The effect of the core size on the structure and chirality of self-assembled molecular networks was investigated using two aromatic carboxylic acid derivatives with frameworks displaying C_{3h} symmetry, triphenylene derivative **H3TTCA** and dehydrobenzo[12]annulene (DBA) derivative **DBACOOH**, each having three carboxy groups per molecule. Scanning tunneling microscopy observations at the 1-heptanoic acid/graphite interface revealed **H3TTCA** exclusively forming a chiral honeycomb structure, and **DBACOOH** forming three structures (type I, II, and III structures) depending on its concentration and whether the system is subjected to annealing treatment. Hydrogen bonding interaction patterns and chirality were carefully analyzed based on a modeling study using molecular mechanics simulations. Moreover, **DBACOOH** forms chiral honeycomb structures through the co-adsorption of guest molecules. Structural diversity observed for **DBACOOH** is attributed to its relatively large core size, with this feature modulating the balance between molecule–molecule and molecule–substrate interactions.

Introduction

Structural control over self-assembled molecular networks (SAMNs) spontaneously formed by organic molecules on solid surfaces in ultrahigh vacuum (UHV) conditions and at liquid/solid interfaces through non-covalent interactions is of interest owing to corresponding potential applications in nanotechnology.[1–4] In particular, supramolecular chirality of SAMNs is a subject of keen interest in relation to the development of chiral sensors and catalysts through chiral molecular recognition on SAMNs.[5–7] In structural designs of SAMNs, various non-covalent interactions such as van der Waals,[8] hydrogen bonding,[9] coordination bonding,[10,11] and halogen bonding interactions have been employed.[12] Of them, the hydrogen bonding interaction is the most widely used for the construction of SAMNs because of its strength and directionality.[9] Scanning tunneling microscopy (STM) is a useful tool for characterizing SAMNs with a submolecular resolution both at surfaces in UHV conditions and at the liquid/solid interfaces.[13,14]

Dimeric pairs of aromatic carboxylic acids formed each by complementary hydrogen bonding interactions between the carboxy groups have been extensively used in the design of molecular packing structures in three-dimensional (3D) space because of their directionality and selectivity (Fig. 1(a)).[15–17] This hydrogen bonding interaction can also be used in two-dimensional space to construct SAMNs on surfaces both in UHV and interfacial conditions.[18] Many such investigations have been performed in particular under ambient interfacial conditions.[18–20] Trigonal aromatic molecules having each three carboxy groups are ideal molecular building blocks for constructing porous SAMNs displaying hexagonal periodicity.[21] Lackinger and coworkers reported systematic studies on structural control of SAMNs at the liquid/solid interfaces using trimesic acid (**TMA**) and 1,3,5-benzenetribenzoic acid (**BTB**), which are aromatic carboxylic acid derivatives having molecular frameworks displaying D_{3h} symmetry (and have substitutions at the 1,3,5-positions of the central benzene rings, Fig. 1(b)).[22–25] **TMA** is the smallest such molecule that forms honeycomb (chicken-wire) and flower structures at the liquid/graphite interfaces, depending on its concentration and the identity of the solvent.[20,23] In the honeycomb structure, the **TMA** molecules are connected by complementary-type ($R_2^2(8)$) hydrogen bonding interactions between the two carboxy groups, whereas in the flower structure, the **TMA** molecules are connected by both complementary-type ($R_2^2(8)$) and cyclic-type ($R_3^3(12)$) hydrogen bonding interactions, with the cyclic-type interaction formed by three carboxy groups (Fig. 1(a)). The size of the

[a]*Department of Applied Chemistry, School of Science and Technology, Meiji University, 1-1-1 Higashimita, Tama-ku, Kawasaki, 214-8571, Japan. E-mail: tahara@meiji.ac.jp*
[b]*Division of Chemistry, Graduate School of Engineering Science, Osaka University, 1-3 Machikaneyama, Toyonaka, Osaka 560-8531, Japan*

† Electronic supplementary information (ESI) available: Additional STM images, STM image analysis, details of MM calculations. See DOI: https://doi.org/10.1039/d3ra05762c

aromatic core has impacts on SAMN formation.[20] **BTB** is a larger molecule having a framework displaying D_{3h} symmetry, and in which the 1,3,5-position hydrogens of the central benzene ring are substituted with 4-carboxyphenyl groups (Fig. 1(b)); the molecule forms a porous honeycomb as well as oblique structures, and a non-porous close-packed structure at the liquid/graphite interfaces.[20,25] In the oblique structure, a hydrogen bonding interaction between the carboxy group and a hydrogen atom of the benzene ring would be formed in addition to the complementary-type ($R_2^2(8)$) hydrogen bonding interactions between the carboxy groups (Fig. 1(a)). Moreover, large molecules based on a **TMA** motif also produce various porous SAMNs.[26–32] In some of these SAMNs, guest molecules fit into the pores are co-adsorbed.[27,29] Moreover, a non-porous SAMN sometimes shows a structural rearrangement in response to the addition of guest molecules through co-adsorption.[33] Recent work has focused on the adaptability of these SAMNs to external stimuli such as heat,[34] to an external electric field,[35–37] and to a combination of these stimuli and additives.[33,38–41] Nevertheless, despite the many studies on **TMA** and its expanded motifs displaying D_{3h} symmetry, only a few studies have been reported on SAMNs having molecular frameworks displaying C_{3h} symmetry.[42–44] The SAMN formation and guest co-adsorption of the simplest molecule having a molecular framework displaying C_{3h} symmetry, namely triphenylene-2,6,10-tricarboxylic acid (**H3TTCA**), have been reported (Fig. 1(c)).[43,44] However, to the best of our knowledge, there has to date never been reported a study on the effect of core size on the formation of SAMNs using a planar molecule having the molecular framework displaying C_{3h} symmetry. Understanding the effect of symmetry group reduction and size modulation of the molecular building blocks on the formation of SAMNs is important for the establishment of 2D crystal engineering (Fig. 1(a) and (c)).

Adsorption of organic molecules onto a surface often generates single-point molecular chirality even for achiral molecules in 3D space because of symmetry group reduction.[45–48] The aromatic carboxylic acid derivatives having molecular frameworks displaying D_{3h} symmetry would remain achiral on the surface at the single-molecule level (Fig. 2(a) and (c)). Here the orientation of the carboxy groups on a surface is ignored because it does not influence complementary hydrogen bonding interactions between the carboxy groups ($R_2^2(8)$ and $R_3^3(12)$) (Fig. 1(a) and 2). While the molecules displaying D_{3h} symmetry are achiral at the single-molecule level, their SAMNs sometimes adopt one of the chiral plane groups (*P1*, *P2*, *P3*, *P4*, and *P6*).[49] For instance, the domains of the honeycomb structures of **TMA** and **BTB** are chiral, and this supramolecular chirality is distinguished only by the domain orientations with respect to the graphite lattice underneath (Fig. 2(e)). Specifically, the supramolecular chirality is determined by the sign (positive or negative) of α angle between the unit cell vector of the honeycomb structure and the nearest normal to the main symmetry axes of graphite (Fig. 2(e)). On the other hand, the achiral aromatic carboxylic acid derivatives having molecular frameworks displaying C_{3h} symmetry (Fig. 1(c) and 2(b)) show single-point molecular chirality on the surface. We defined this single-point chirality as an *R*-type or *L*-type (Fig. 2(d)). The chiral

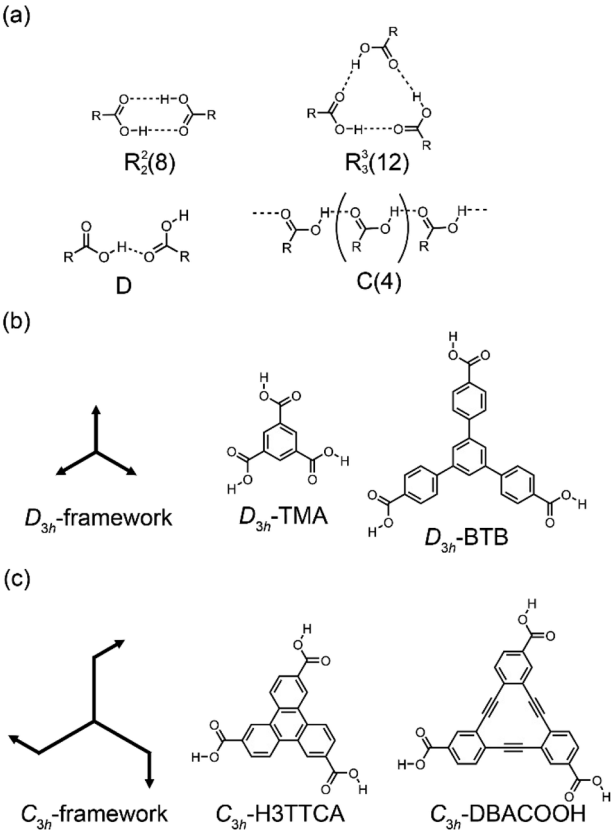

Fig. 1 (a) Four motifs of hydrogen bonding interactions (D, $R_2^2(8)$, C(4), and $R_3^3(12)$) of carboxy groups. The cyclic hydrogen bonding motif is represented by $R_y^x(Z)$, where *x* and *y* are the numbers of H-bond donors and acceptors, respectively, and *Z* is the total number of atoms involved in the hydrogen bonding interactions. (b) Chemical structures of **TMA** and **BTB**, which are aromatic carboxylic acid derivatives having molecular frameworks displaying D_{3h} symmetry. (c) Chemical structures of **H3TTCA** and **DBACOOH**, which are aromatic carboxylic acid derivatives having molecular frameworks displaying C_{3h} symmetry.

R- or *L*-type molecule appears with equal probability on the surface. Assembling such a racemic mixture on a surface can lead to two outcomes: the formation of separate domains of homochiral structures (2D-conglomerate) or the formation of an achiral structure composed of equal amounts of both chiral molecules in the domain (2D-racemate).[50,51] The supramolecular chirality of the domains in 2D-conglomerates could be distinguished by the orientation of each molecule (*R*- or *L*-type) as well as the relative orientation of the domains with respect to the substrate lattice (Fig. 2(f)). These SAMNs display one of the chiral 2D plane groups. In the case of the 2D-racemates, the SAMNs can display the chiral as well as achiral plane groups.[50,51] When the 2D-racemate displays one of the chiral plane groups, the domain handedness is defined by its relative orientation with respect to the substrate lattice. Even for the simplest case of a molecule having the molecular framework displaying C_{3h} symmetry, a detailed analysis of the chirality of the SAMNs has, to the best of our knowledge, not yet been reported (Fig. 1(c)).[42–44] Therefore, addressing supramolecular chirality aspects of these SAMNs is also an intriguing subject.[49]

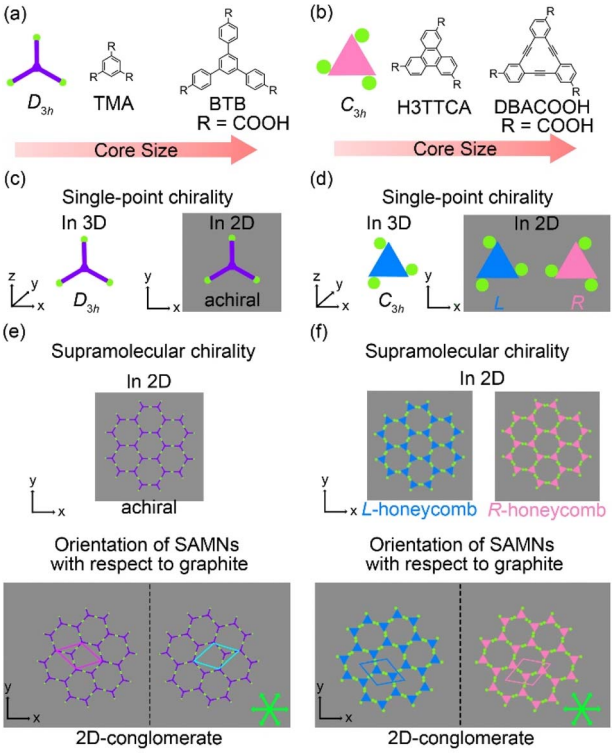

Fig. 2 (a) Schematic representation and chemical structures of TMA and BTB having frameworks displaying D_{3h} symmetry. (b) Schematic representation and chemical structures of H3TTCA and DBACOOH having frameworks displaying C_{3h} symmetry. (c) Schematic drawings representing the single-molecule chirality of a D_{3h}-symmetric aromatic molecule in 3D space and 2D space. (d) Schematic drawings representing the single-molecule chirality of a C_{3h}-symmetric aromatic molecule in 3D space and 2D space. (e) Schematic drawings representing the supramolecular chirality of a honeycomb structure formed by D_{3h}-symmetric molecules on a surface. (f) Schematic drawings representing the supramolecular chirality of a honeycomb structure formed by C_{3h}-symmetric molecules on a surface. Gray panels in (c)–(f) represent graphite surfaces. Green arrows mark the main symmetry axes of the graphite substrate. The dashed lines in (e) and (f) represent mirror planes.

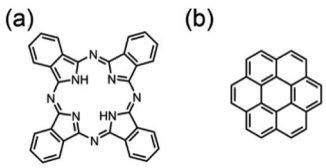

Fig. 3 Chemical structures of the guest molecules (a) phthalocyanine and (b) coronene.

In this context, we herein investigated the effect of the core size on the structure and chirality of SAMNs using two aromatic carboxylic acids having frameworks displaying C_{3h} symmetry, namely **H3TTCA** and dehydrobenzo[12]annulene (DBA) derivative **DBACOOH**, each having three carboxy groups per molecule, at the 1-heptanoic acid (1-HA)/graphite interfaces. STM observations revealed an exclusive formation of a chiral honeycomb structure by **H3TTCA**, while **DBACOOH** shows structural polymorphism, with the structure formed depending on its solute concentration and whether the system is subjected to annealing treatment. **DBACOOH** was found to form three types of structures, denoted here as type I, II, and III structures. The structural diversity observed for **DBACOOH** is attributed to its relatively large core size, a feature modulating the balance between molecule–molecule and molecule–substrate interactions. We also investigated guest co-adsorption in the SAMNs of **DBACOOH**. Chiral honeycomb structures are formed upon the addition of the guest molecule, coronene or phthalocyanine (Fig. 3 and S1†). The guest co-adsorption is essential for the formation of the honeycomb structures by **DBACOOH**.

Results and discussion

The synthesis of **H3TTCA** and **DBACOOH** was reported elsewhere.[52,53] 1-HA was used as a solvent for the preparation of sample solutions. To investigate the dependence of the structure on solute concentration, the solute concentrations from 1.0×10^{-6} to 1.5×10^{-4} M were tested. The sample solution (15 or 40 μL, the latter for annealing treatment) was poured into a liquid cell placed on a freshly cleaved surface of a highly oriented pyrolytic graphite to prepare SAMNs at the interface. In order to anneal a sample, the cell containing the sample was heated at 80 °C in a sealed oven for 3 h and then allowed to cool to room temperature. All STM observations of the SAMNs were then conducted at the 1-HA/graphite interfaces at room temperature.

The **H3TTCA** molecules were observed to exclusively form a honeycomb structure at the 1-HA/graphite interface at all solute concentrations (Fig. 4 and S2†). Since π-conjugated cores were observed as bright features in STM images because of their higher tunneling efficiency,[54,55] bright triangles composed of three small doughnut-like features were assigned to the π-conjugated cores of **H3TTCA**. The honeycomb structure consists of the **H3TTCA** molecules with two different orientations of 60° (Fig. S3†). In the STM images, short rod-like features were observed at the periphery of the hexagonal pore, and these were attributed to co-adsorbed 1-HA molecules. The unit cell parameters of the honeycomb structure were measured to be $a = b = 2.3 \pm 0.1$ nm and $\gamma = 60.1 \pm 0.4°$ (Fig. 4(a)), values consistent with those in the previous reports.[43,44] The honeycomb structure adopts the chiral *P6* symmetry group. The distance between the centers of the benzene rings of adjacent **H3TTCA** molecules was measured to be 0.8 ± 0.1 nm. Based on the unit cell parameters and this intermolecular distance, the network models were optimized using molecular mechanics (MM) simulation (COMPASS force field). In the optimized model, shown in Fig. 4(b), the O···H distance in the dimeric pair of carboxy groups between adjacent **H3TTCA** molecules is 0.175 nm,[56,57] supporting the formation of complementary-type hydrogen bonding interactions ($R_2^2(8)$). The honeycomb structure consists of only one enantiomer (*R* or *L*-**H3TTCA**, Fig. 4(d) and (e)), thus indicating the honeycomb structure to be chiral (*R* or *L*). This chirality is identical throughout the domains. The two enantiomorphic *R* and *L* domains were identified by the negative and positive signs of the value of the α angle between

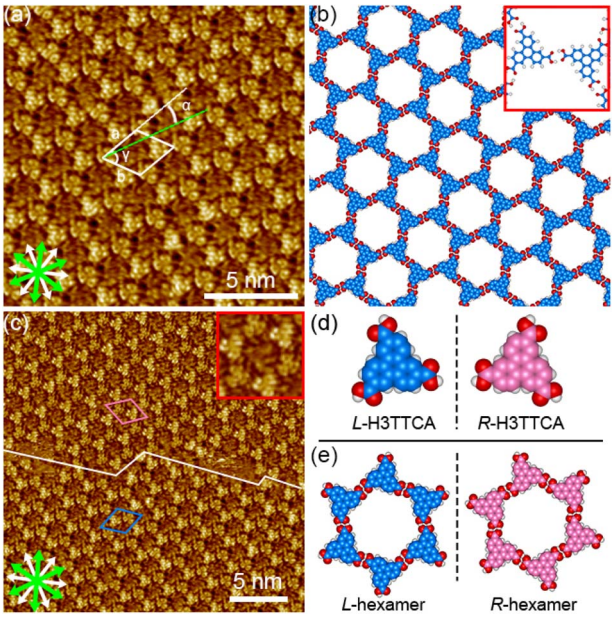

Fig. 4 SAMNs formed by **H3TTCA** at the 1-HA/graphite interface. (a) STM image showing the honeycomb structure produced using a solute concentration of 2.0×10^{-5} M (tunneling parameters: I_{set} = 230 pA and $V_{bias} = -0.56$ V) and (b) a corresponding molecular model optimized by performing an MM calculation. Inset in (b) shows a complementary hydrogen bonding interactions between the carboxy groups ($R_2^2(8)$). White and green arrows mark the main symmetry axes of the graphite substrate underneath and the in-plane directions normal to the main symmetry axes of the graphite substrate underneath, respectively. (c) STM image showing domains and the boundary between them in the chiral honeycomb structure produced using a solute concentration of 2.0×10^{-5} M (tunneling parameters: I_{set} = 230 pA and $V_{bias} = -0.61$ V). Inset in (c) shows a digitally zoomed image of a single hexagonal pore of the honeycomb structure highlighting the rod-like features described in the main text. (d) Models showing on-surface chirality (*L* or *R*) of **H3TTCA** at the single-molecule level. (e) Models of hydrogen-bonded chiral hexamers (*L* or *R*-hexamer) of the **H3TTCA** molecules.

the short unit cell vector *a* and the one nearest to normal to the main symmetry axes of graphite. The $|\alpha|$ average angle value was determined to be $12 \pm 1°$ (Fig. 4(c) and S4†). Both enantiomorphous domains appear with equal probability, confirming formation of a 2D-conglomerate (Fig. S4†).

Next, we investigated the SAMNs of **DBACOOH** at the 1-HA/graphite interface. **DBACOOH** forms three different SAMNs depending on its concentration and whether annealing is carried out (Fig. S5†). At solute concentrations from 1.0×10^{-6} to 1.0×10^{-5} M, type I and II structures were observed (Fig. 5 and 6). After an annealing treatment, at the same concentration range, a type III structure is formed (Fig. 7). At a solute concentration of 1.5×10^{-4} M, and regardless of whether an annealing treatment is applied, **DBACOOH** forms a non-periodic structure (Fig. S6†) in which the **DBACOOH** molecules adopting various orientations are packed densely on the surface.

In the type I structure, hexagonal and rectangular pores were observed to be arranged in a periodic manner (Fig. 5(b) and (c)). In these pores, we observed dim rod-like features (Fig. 5(c)), attributed to co-adsorbed 1-HA molecules. The unit cell

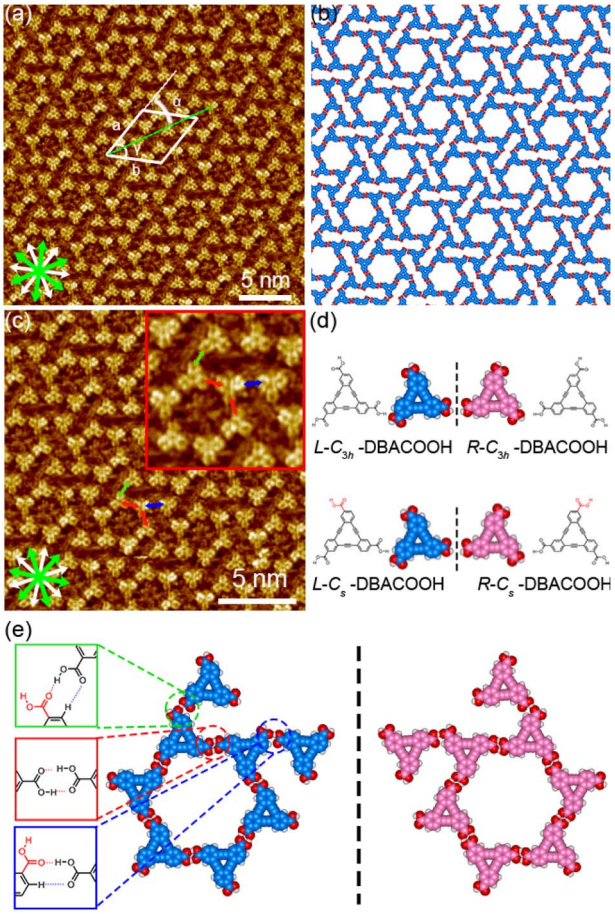

Fig. 5 Type-I-structure SAMNs formed by **DBACOOH** at the 1-HA/graphite interface. (a) STM image showing the type I structure produced using a solute concentration of 6.0×10^{-6} M (tunneling parameters: I_{set} = 200 pA and $V_{bias} = -0.39$ V) and (b) a corresponding molecular model optimized by performing an MM calculation. White and green arrows are the main symmetry axes of the graphite substrate underneath and the in-plane directions normal to those, respectively. (c) STM image showing the type I structure produced using a solute concentration of 3.0×10^{-6} M (tunneling parameters: I_{set} = 200 pA and $V_{bias} = -0.39$ V). Red arrow indicates the distance between the centers of the nearest benzene rings of adjacent **DBACOOH** molecules in the cyclic hexamer. Blue and green arrows each indicate the distance between the center of a benzene ring in the hexagonal hexamer and the center of the benzene ring in another adjacent **DBACOOH** molecule located in between the cyclic hexamers. Note that two structurally independent **DBACOOH** molecules have been identified to be located in between the cyclic hexamers in this structure, with the blue arrow connecting to one of these molecules, and the green arrow to the other. Inset in (c) shows a digitally zoomed image. (d) Models showing the on-surface chirality and conformation of **DBACOOH** at the single-molecule level. (e) Models of eight independent **DBACOOH** molecules (six in the hexamer and two between hexamers) connected through hydrogen bonding interactions of the carboxy groups. Square frames show the chemical structures of three modes of hydrogen bonding interactions between the carboxy groups. Color codes in the square frames correspond to the three different intermolecular distances indicated by the arrows in (c). The red and blue dotted lines in insets of (e) indicate hydrogen bonding interactions between the carbonyl groups of **DBACOOH** molecules and hydrogen bonding interactions between the carbonyl groups and the hydrogen atom of the benzene ring, respectively.

parameters for the type I structure were measured to be $a = b = 5.12 \pm 0.06$ nm and $\gamma = 59.9 \pm 0.4°$. And the chiral *P6* group was identified to be the plane group of the type I structure, when two DBA molecules located between the cyclic hexamers are not regarded as asymmetry units. In this type I structure, eight structurally distinct **DBACOOH** molecules were identified in the unit cell: six of them arranged in a hexamer and two located between hexamers. The distance between the centers of nearest benzene rings of adjacent **DBACOOH** molecules located at the vertices of a hexagonal pore was measured to be 0.70 ± 0.04 nm (red arrow in Fig. 5(c)). And for each of the two non-hexamer **DBACOOH** molecules, the distance between either **DBACOOH** molecule and the nearest **DBACOOH** molecule in the hexamer—specifically the distance between the centers of the nearest benzene rings—happened to be about the same, namely 0.9 ± 0.1 nm, despite their geometries being structurally inequivalent (blue and green arrows in Fig. 5(c)). The difference in the intermolecular distances between that within the hexamer and that between the hexamer and outside the hexamer suggested two different hydrogen bonding interaction modes. Accordingly, a network model was carefully constructed using MM simulation based on the unit cell parameters and these intermolecular distances (Fig. 5(b)). The hexagonal pore consisting, as described above, of the molecules having two different orientations of 60° suggests the formation of a homochiral *L* or *R* hexamer (Fig. 2(f)). To assess the chirality of remaining **DBACOOH** molecules located in between the hexamers, we modeled three possible molecular arrangements: (1) one having the same chirality of the molecules in the hexamer (Fig. S7(a)†), and (2) the other two molecules having the opposite chirality (Fig. S7(b) and (c)†). The network model consisting of the same chiral orientation nicely matches the experimental results. While the orientation of the carboxy groups could not be determined from the STM images, we considered that, to maximize the number of hydrogen bonding interactions, the DBA molecules in the hexamer adopt a C_s symmetry group with a different orientation for one of the three carboxy groups. The MM simulation yields two mean intermolecular O···H distances, namely 0.172 and 0.188 nm, for the two different types ($R_2^2(8)$ and D types) of hydrogen bonding interactions between the carboxy groups (Fig. 5(d) and (e)).[56,57] Moreover, in the D type interaction, there is a weak hydrogen bonding interaction between a hydrogen atom of the benzene ring and an oxygen atom of the carboxy group (0.249 nm) (Fig. 5(d) and (e)).[56,58] Further details on the network modeling are described in ESI (Fig. S7†). The type I structure was observed to be chiral throughout the domains, and this chirality could be differentiated by the sign (positive or negative) of the α angle value (*R* or *L*). An $|\alpha|$ average angle value of $27.5 \pm 0.6°$ was measured (Fig. S8†). Both chiral domains appear with equal probability and thus the type I structure is regarded as a 2D-conglomerate.

The type II structure was observed to contain a narrow rectangular pore, and to be composed of four independent **DBACOOH** molecules with different orientations. Our results indicated unit cell parameters of $a = 2.8 \pm 0.1$ nm, $b = 4.9 \pm 0.1$ nm, and $\gamma = 54 \pm 1°$ and a chiral *P2* plane group for the type II structure. The distances between the benzene rings of the adjacent independent **DBACOOH** molecules were measured to be 0.8 ± 0.1 nm, 0.9 ± 0.1 nm, and 0.7 ± 0.1 nm, respectively (red, green, and blue arrows in Fig. 6(a)). A network model optimized by carrying out an MM simulation based on the unit cell parameters and these intermolecular distances are shown in Fig. 6(b).

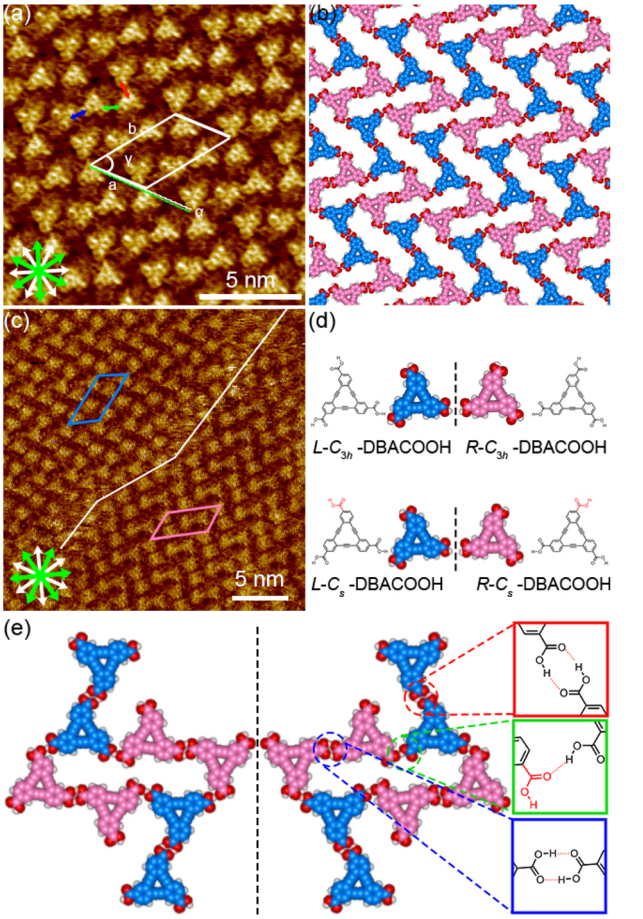

Fig. 6 Type-II-structure SAMNs formed by **DBACOOH** at the 1-HA/graphite interface. (a) STM image showing the type II structure produced using a solute concentration of 6.0×10^{-6} M (tunneling parameters: $I_{set} = 200$ pA and $V_{bias} = -0.39$ V) and (b) corresponding molecular model optimized by performing an MM calculation. White and green arrows are the main symmetry axes of the graphite substrate underneath and the in-plane directions normal to those, respectively. (c) STM image showing the type II structure produced using a solute concentration of 3.0×10^{-6} M (tunneling parameters: $I_{set} = 230$ pA, $V_{bias} = -0.47$ V). Red, blue, and green arrows indicate the distances between the centers of the indicated benzene rings of adjacent **DBACOOH** molecules. The white line marks a domain boundary. (d) Models showing the on-surface chirality and conformation of **DBACOOH** at the single-molecule level. (e) Molecular models of the rectangular pore formed by eight **DBACOOH** molecules connected through intermolecular hydrogen bonding interactions between the carboxy groups. Square frames show the chemical structures of two hydrogen bonding modes between the carboxy groups. Color codes in the square frames correspond to the three different intermolecular distances indicated by the arrows in (a). The red dotted lines in insets of (e) indicate hydrogen bonding interactions between the carbonyl groups of **DBACOOH** molecules.

Of the three possible network structures with a different combination of homo- or heterochiral molecular orientations—namely the homochiral (*R*,*R*,*R*,*R* or *L*,*L*,*L*,*L*) structure and heterochiral (*R*,*R*,*L*,*L* or *L*,*L*,*R*,*R*) and (*R*,*R*,*R*,*L* or *L*,*L*,*L*,*R*) structures (Fig. S9†)—the heterochiral (*R*,*R*,*L*,*L* or *L*,*L*,*R*,*R*) structure was found to be the one in good agreement with the π-core positions in the STM images (Fig. 6(d) and (e)). We assumed in the MM model the formation of a maximum number of intermolecular hydrogen bonding interactions between the carboxy groups (see ESI†). The four inequivalent **DBACOOH** molecules (*R*-C_{3h}, *R*-C_s, *L*-C_{3h} and *L*-C_s symmetry) are connected through the two types ($R_2^2(8)$ and D types, Fig. 6(e)) of hydrogen bonding interactions with the two mean O···H distances of 0.172 nm and 0.179 nm.[56,57] Despite the type II structure containing equal numbers of the chiral *R* and *L* molecules, domains having two different orientations with respect to the graphite lattice underneath were identified. This handedness was again determined by the sign of the α angle (+ or − for *R* or *L*). The $|\alpha|$ average angle value was measured to be 0.2 ± 0.3° (Fig. 6 and S10†). Both enantiomorphous domains appear with equal probability.

The type III structure appears exclusively after annealing treatment using the sample solutions at concentrations from 3.0×10^{-6} to 1.0×10^{-5} M (Fig. 7(a)). The structural change indicates the type III structure to be a thermodynamically favored phase relative to the type I and II structures. In the type III structure, the **DBACOOH** molecules were observed to be densely arranged in a linear fashion. Our results showed unit cell parameters of $a = 1.5 \pm 0.1$ nm, $b = 4.5 \pm 0.1$ nm, and $\gamma = 70 \pm 1°$ and the chiral *P2* symmetry group for this type III structure. The distances between the benzene rings of the adjacent independent **DBACOOH** molecules were measured to be 0.7 ± 0.1 nm, 0.9 ± 0.1 nm, and 0.8 ± 0.1 nm, respectively (red, green, and blue arrows in Fig. 7(a)). Two possible structures, a homochiral alignment consisting of the molecules with the *R*- or *L*-orientation and a heterochiral alignment consisting of the molecules with both *R*- and *L*-orientations, were modeled (Fig. S11†). The homochiral alignment optimized by performing an MM simulation was found to nicely match the positions of each triangular π-core of **DBACOOH** in the STM image (Fig. 7(b)). In the MM model, there is one type of hydrogen bonding interaction (D type) between the carboxy groups (Fig. 7(d) and (e)), with a mean O···H distance of 0.173 nm.[56,57] The supramolecular chirality of the type III structure was also determined by the sign (positive or negative) of the α angle (*R* or *L*, Fig. 7(c)), with the $|\alpha|$ average angle value measured to be 13 ± 1° (Fig. S12†). As both chiral domains appear with equal probability, the type III structure is concluded to be a 2D-conglomerate.

Structural rearrangement of **H3TTCA** SAMNs upon addition of guest molecules such as phthalocyanine and coronene has been reported.[43,44] In this context, we investigated the effect of these guest molecules on the SAMN formation of **DBACOOH**.

First phthalocyanine, with its large square π-core, was tested (Fig. 3(a) and S1†). We tested various pre-mixed solutions of **DBACOOH** and phthalocyanine with different guest/host (G/H) molar ratios but in which the concentration of **DBACOOH** was kept constant at 1.0×10^{-5} M. Extended domains of the honeycomb structure were observed at exclusively a G/H ratio of 5/1 (Fig. 8(a) and S13†). Inspection of the STM image of this SAMN showed fuzzy bright circular features at the hexagonal pores. We attributed these bright features to co-adsorbed phthalocyanine molecules (Fig. 8(c) and (d)). The fuzzy appearance is attributed to the lateral mobility of the guest molecules at the pore. Also, distorted hexagonal pores were observed at the domain borders, and a square bright feature was occasionally observed in these distorted pores (Fig. 8(c) and (d)). This square appearance is attributed to size complementarity between the guest molecule and distorted pore. Unit cell parameters for this honeycomb structure (*P6* group) were measured to be $a = b = 2.91 \pm 0.07$ nm and $\gamma = 60.1 \pm 0.4°$. A corresponding molecular model optimized by performing an MM simulation based on experimental data is shown in Fig. 8(b). This optimization shows the **DBACOOH** molecules adopting two orientations with a difference of 60°, suggesting

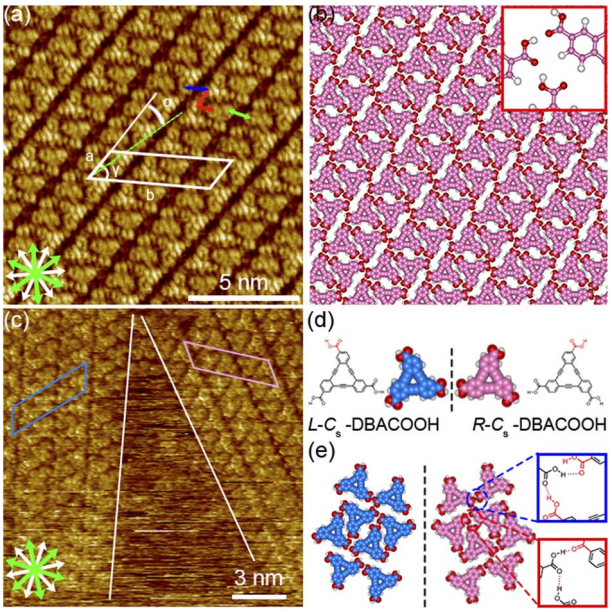

Fig. 7 Type-III-structure SAMNs formed by **DBACOOH** at the 1-HA/graphite interface. (a) STM image showing the type III structure produced using a solute concentration of 6.0×10^{-6} M (tunneling parameters: $I_{set} = 200$ pA and $V_{bias} = -0.39$ V) and (b) corresponding molecular model optimized by performing an MM calculation. The red, blue, and green arrows indicate the distance between the centers of the nearest benzene rings of adjacent **DBACOOH** molecules. White and green arrows are the main symmetry axes of the graphite substrate underneath and the in-plane directions normal to those, respectively. (c) STM image showing the type III structure produced using a solute concentration of 3.0×10^{-6} M (tunneling parameters: $I_{set} = 200$ pA and $V_{bias} = -0.39$ V). (d) Models showing the on-surface chirality of **DBACOOH** at the single-molecule level. (e) Molecular models of the two chiral **DBACOOH** pairs connected by hydrogen bonding interactions between the carboxy groups. Square frames show the chemical structures of hydrogen bonding mode between the carboxy groups. Color codes in the square frames correspond to the two different intermolecular distances indicated by the arrows in (a). The red dotted lines in the square frames of (e) indicate hydrogen bonding interactions between the carbonyl groups of **DBACOOH** molecules.

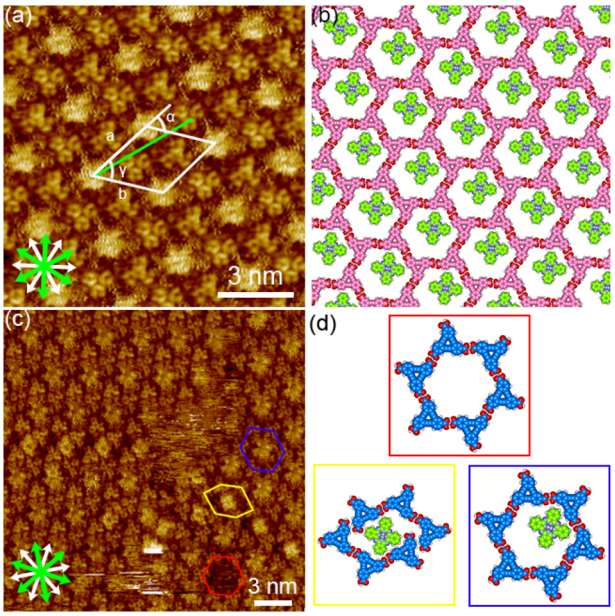

Fig. 8 SAMNs formed by a mixture of **DBACOOH** and phthalocyanine at the 1-HA/graphite interface. (a) STM image showing the honeycomb structure produced using a mixture of **DBACOOH** (1.0×10^{-5} M) and phthalocyanine (1.1×10^{-4} M, tunneling parameters: $I_{set} = 200$ pA and $V_{bias} = -0.61$ V) and (b) corresponding molecular model optimized by performing an MM calculation. (c) STM image showing the honeycomb structure with co-adsorbed phthalocyanine molecules produced using a mixture of **DBACOOH** (1.0×10^{-5} M) and phthalocyanine (1.1×10^{-4} M, tunneling parameters: $I_{set} = 210$ pA and $V_{bias} = -0.39$ V). Red, yellow, and blue hexagons mark a vacant pore, a distorted pore with an immobilized guest molecule, and a pore with a mobile phthalocyanine molecule. (d) Molecular models of three different hexagonal pores optimized by performing MM calculations. The models surrounded by the squares with different color correspond the molecular arrangements in the hexagons with the same color in image (c).

the formation of a homochiral hexamer. The complementary hydrogen bonding interactions of the $R_2^2(8)$ type between the carboxy groups sustain the cyclic hexamer (Fig. 8(b)). An O···H distance of 0.173 nm is in the MM model. The formation of *L versus R* supramolecular chirality was discerned by noting the sign (positive or negative) of the α angle. In the current work on **DBACOOH** with phthalocyanine, the $|\alpha|$ average angle value was measured to be $17 \pm 1°$ (Fig. S14†). This result is indicative of the honeycomb structure being a 2D-conglomerate. The two-component honeycomb structure was transformed into a type III structure over the activation barrier for the structural rearrangement upon annealing (Fig. S13†). This result implied the two-component honeycomb structure to be a kinetically trapped phase.

Next, coronene with its D_{6h} symmetry was tested as a guest molecule (Fig. 3(b) and S1†). Note the symmetry of this molecule fitting that of the pore, but its size being smaller than that of the pore. Extended domains of the honeycomb structure were observed at exclusively a G/H ratio of 10/1 (Fig. 9(a) and S15†). Fuzzy features with different levels of brightness were observed at the pore, indicating the co-adsorption of coronene molecules (Fig. 9(c) and (d)). The diameter of the brightest feature in the pore was measured to be 1.9 ± 0.1 nm, a value corresponding to twice the coronene diameter. Therefore, these features were attributed to two or three co-adsorbed coronene molecules. Lackinger and coworkers attributed the different levels of brightness of the co-adsorbed coronene molecules in the honeycomb structures of **TMA** and **BTB** to different numbers of co-adsorbed coronene molecules[59] and/or to lateral mobility of the guest molecules in the pore.[60] The coronene molecules with lateral dynamics in the pore would reflect their appearance in the STM images. Moreover, fuzzy oval features were observed in the distorted hexagonal pores at the domain boundaries (Fig. 9(c) and (d)). Lengths of 1.8 ± 0.1 nm and 1.1 ± 0.1 nm were measured for, respectively, the long and short sides of the fuzzy oval features, indicating these features to be two co-adsorbed coronene molecules. Our measurements indicated unit cell parameters of $a = b = 2.91 \pm 0.08$ nm and $\gamma = 60.1 \pm 0.6°$ for this honeycomb structure. An MM-optimized network model based on the above result is shown in Fig. 9(b). Moreover, the two-component honeycomb structure was also found to be

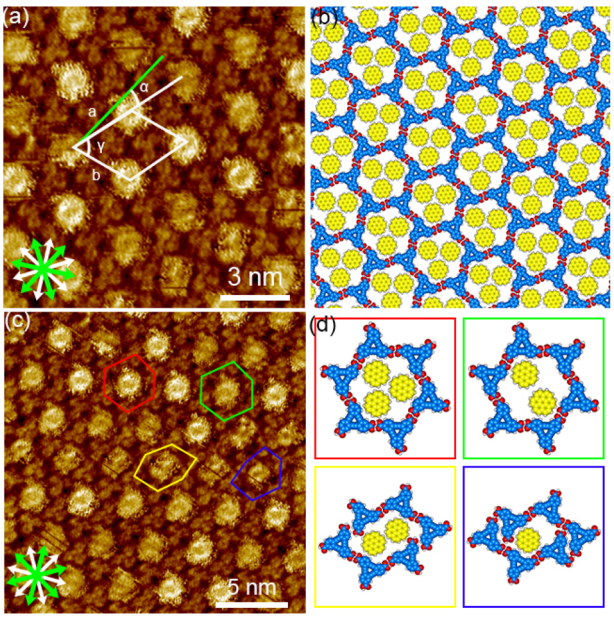

Fig. 9 SAMNs formed by a mixture of **DBACOOH** and coronene at the 1-HA/graphite interface. (a) STM image showing the honeycomb structure of **DBACOOH** with co-adsorbed coronene molecules and produced using a mixture of **DBACOOH** (1.0×10^{-5} M) and coronene (1.0×10^{-4} M, tunneling parameters: $I_{set} = 200$ pA and $V_{bias} = -0.64$ V) and (b) corresponding molecular model optimized by performing an MM calculation. (c) STM image showing the honeycomb structure of **DBACOOH** with co-adsorbed coronene molecules and produced using a mixture of **DBACOOH** (1.0×10^{-5} M) and coronene (1.0×10^{-4} M, tunneling parameters: $I_{set} = 200$ pA and $V_{bias} = -0.61$ V). Red and green hexagons mark, respectively, the brightest and dimmer fuzzy pores. Yellow and blue hexagons mark two different distorted pores appearing at the domain boundaries. (d) Molecular models of the four different hexagonal pores constructed from MM calculations. The models surrounded by the squares with different color correspond the molecular arrangements in the hexagons with the same color in image (c).

Table 1 Estimated non-bonding interaction energies (kcal mol^{-1} nm^{-2}) of the SAMNs of **H3TTCA** and **DBACOOH** on a bilayered graphene sheet from MM simulations

Compound	Structure	N^a	Molecular density (nm^{-2})	$E_{total}{}^b$ (kcal mol^{-1} nm^{-2})	$E_{mol-mol}{}^c$ (kcal mol^{-1} nm^{-2})	$E_{mol-sub}{}^d$ (kcal mol^{-1} nm^{-2})
H3TTCA	Honeycomb	2	0.38	−30.8	−12.1	−18.6
DBACOOH	Honeycomb[e]	2	0.27	−17.5	−1.5	−15.9
DBACOOH	Type I	8	0.35	−21.6	−0.8	−20.8
DBACOOH	Type II	4	0.39	−23.0	0.2	−23.2
DBACOOH	Type III	4	0.56	−39.9	−2.6	−37.3

[a] Number of the indicates molecules per unit cell. [b] Non-bonding interaction energy of the whole system including the substrate (bilayered graphene sheets). [c] Non-bonding interaction energy obtained from a single-point energy calculation of the molecules without the substrate. [d] Non-bonding interaction energy between the molecules and substrate, calculated using the equation $E_{mol-sub} = E_{total} - E_{mol-mol}$. [e] A honeycomb structure of **DBACOOH** is a hypothetical model construed for a comparison.

Table 2 Intermolecular non-bonding interaction energies (kcal mol^{-1} nm^{-2}) for host–guest systems each on a bilayered graphene sheet and calculated from MM simulations using the COMPASS force field

Structure	Guest molecule	E_{total} (kcal mol^{-1} nm^{-2})	$E_{host}{}^a$ (kcal mol^{-1} nm^{-2})	$E_{guest}{}^b$ (kcal mol^{-1} nm^{-2})	$E_{host-guest}{}^c$ (kcal mol^{-1} nm^{-2})
Honeycomb	One phthalocyanine	−40.0	−17.4	−22.3	0.3
Honeycomb	Three coronenes	−26.4	−17.3	−7.9	1.2

[a] E_{host} values were obtained by performing single-point energy calculations for the host–guest systems in their optimized geometries without guest molecule(s). [b] E_{guest} values were obtained by performing single-point energy calculations for the host–guest systems in their optimized geometries without the host networks. [c] Calculated using the equation $E_{host-guest} = -(E_{total} - E_{host} - E_{guest})$.

chiral, and its handedness to be determined by the sign (positive or negative) of the α angle (R or L). The $|\alpha|$ average angle value was measured to be 17 ± 1° (Fig. S16†). This two-component honeycomb structure also transformed into the type III structure through desorption of the guest molecules upon annealing (Fig. S15†). This two-component honeycomb structure was also concluded to be a kinetically trapped phase.

H3TTCA forms only the chiral honeycomb structure, regardless of the solute concentration, and does so as a 2D-conglomerate. In contrast, **DBACOOH** shows structural polymorphism, with the four structures depending on solute concentration, whether the system is subjected to annealing, and the presence of the guest molecules. The type I and III structures as well as the two-component honeycomb structures are 2D-conglomerates. The type II structure is a 2D-racemate in terms of the composition of the L and R-molecules within the domain, while the domains show two chiral orientations.

We considered the difference in absorbance abilities of **H3TTCA** and **DBACOOH** to be a possible explanation for the structural polymorphism observed for **DBACOOH** but not for **H3TTCA**. Table 1 summarizes the total energies per unit area (E_{total}) estimated by MM calculations. These calculations indicated the E_{total} value of the honeycomb structure of **H3TTCA** to be lower than that of **DBACOOH**. This result is consistent with the STM observation, which indicates that the **H3TTCA** molecules form the honeycomb structure while the **DBACOOH** molecules do not. This is due to a lower molecular density on the surface for **DBACOOH**. Next, the relative stabilities of the type I, II, and III structures of **DBACOOH** are compared. This comparison shows a small difference in the E_{total} values between the type I and II structures. And on the other hand, the calculations showed a highly negative E_{total} value for the type III structure. This difference between the type III structure and the other structures is attributed to the type III structure having the highest surface molecular density. Again, the highly negative E_{total} value for the type III agrees with the experimental observations. The calculations showed roughly comparable contributions of $E_{mol-sub}$ and $E_{mol-mol}$ to E_{total} for **H3TTCA**, but much greater contributions of the $E_{mol-sub}$ values than of the $E_{mol-mol}$ values to E_{total} for **DBACOOH**. We considered that the enlargement of the core, upon switching from **H3TTCA** to **DBACOOH**, altered the balance of these interactions resulting in the formation of various, yet high-density phases for **DBACOOH**.

Next, we estimated the interaction energies for the host–guest systems of **DBACOOH** from the results of MM simulations (Table 2). The E_{total} values of the honeycomb structures with one co-adsorbed phthalocyanine molecule per pore and three co-adsorbed coronene molecules per pore were calculated to be lower than those of the type I and II structures, consistent with the experimental observations. The calculations indicated a lower E_{total} value for the type III structure than for the honeycomb structure with coronene, results agreeing with the favorable formation of the type III structure upon annealing. The E_{total} values for the honeycomb structure with phthalocyanine and the type III structure are essentially identical. The formation of the type III structure upon annealing would relate

to the factors that were not considered in the MM simulations, such as solvation and wetting energies.

Conclusions

We investigated the structure and chirality of the SAMNs of the C_{3h}-symmetric molecular building blocks **H3TTCA** and **DBA-COOH**, highlighting the effect of the core size. At the 1-HA/graphite interfaces, **H3TTCA** exclusively forms the honeycomb structure which is a 2D-conglomerate. On the other hand, **DBACOOH** forms the type I, type II, and type III structures depending on the solute concentration and whether annealing is applied. The type I and type III structures were observed to consist of two homochiral domains in which the molecules had the same chiral orientation, forming 2D-conglomerates. On the other hand, the type II structure was found to be a 2D-racemate based on its composition. However, all observed structures show handedness with respect to the lattice of the graphite surface underneath. The formation of three structures of **DBA-COOH** is attributed to its extensive molecule–substrate interactions, in turn due to its large core size. The honeycomb structure is kinetically formed for **DBACOOH** upon the addition of the guest molecules and their co-adsorption at the pore. The present study has provided useful information on the effect of the size of the core, in C_{3h}-symmetric aromatic carboxylic acid derivatives, on the formation of SAMNs. We expect this information to be important for further designs and control of the structure and chirality of SAMNs using hydrogen bonding interactions between the carboxy groups.

Conflicts of interest

There are no conflicts to declare.

Acknowledgements

This work was supported by JSPS KAKENHI Grant Number JP20H02553.

Notes and references

1 J. A. A. W. Elemans, S. Lei and S. De Feyter, *Angew. Chem., Int. Ed.*, 2009, **48**, 7298–7333.
2 L. Sosa-Vargas, E. Kim and A.-J. Attias, *Mater. Horiz.*, 2017, **4**, 570–583.
3 D. Cui, J. M. MacLeod and F. Rosei, *Chem. Commun.*, 2018, **54**, 10527–10539.
4 D. P. Goronzy, M. Ebrahimi, F. Rosei, Arramel, Y. Fang, S. De Feyter, S. L. Tait, C. Wang, P. H. Beton, A. T. S. Wee, P. S. Weiss and D. F. Perepichka, *ACS Nano*, 2018, **12**, 7445–7481.
5 T. Kudernac, S. Lei, J. A. A. W. Elemans and S. De Feyter, *Chem. Soc. Rev.*, 2009, **38**, 402–421.
6 X. Zhang, Q. Zeng and C. Wang, *RSC Adv.*, 2013, **3**, 11351–11366.
7 Y. Tobe, K. Tahara and S. De Feyter, *Chem. Commun.*, 2021, **57**, 962–977.
8 K. Tahara, S. Furukawa, H. Uji-i, T. Uchino, T. Ichikawa, J. Zhang, W. Mamdouh, M. Sonoda, F. C. De Schryver, S. De Feyter and Y. Tobe, *J. Am. Chem. Soc.*, 2006, **128**, 16613–16625.
9 A. G. Slater, L. M. A. Perdigão, P. H. Beton and N. R. Champness, *Acc. Chem. Res.*, 2014, **47**, 3417–3427.
10 L. Dong, Z. Gao and N. Lin, *Prog. Surf. Sci.*, 2016, **91**, 101–135.
11 Y.-F. Geng, P. Li, J.-Z. Li, X.-M. Zhang, Q.-D. Zeng and C. Wang, *Coord. Chem. Rev.*, 2017, **337**, 145–177.
12 A. Mukherjee, J. Teyssandier, G. Hennrich, S. De Feyter and K. S. Mali, *Chem. Sci.*, 2017, **8**, 3759–3769.
13 J. P. Rabe and S. Buchholz, *Phys. Rev. Lett.*, 1991, **66**, 2096–2099.
14 S. De Feyter and F. C. De Schryver, *J. Phys. Chem. B*, 2005, **109**, 4290–4302.
15 A. Mukherjee, *Cryst. Growth Des.*, 2015, **15**, 3076–3085.
16 M. K. Corpinot and D.-K. Bucar, *Cryst. Growth Des.*, 2019, **19**, 1426–1453.
17 G. R. Desiraju, *J. Am. Chem. Soc.*, 2013, **135**, 9952–9967.
18 O. Ivasenko and D. F. Perepichka, *Chem. Soc. Rev.*, 2011, **40**, 191–206.
19 K. Rissanen, *Hot Topics in Crystal Engineering*, Elsevier, Oxford, 2021, pp. 1–16.
20 M. Lackinger and W. M. Heckl, *Langmuir*, 2009, **25**, 11307–11321.
21 J. Li, X. Zu, Y. Qian, W. Duan, X. Xiao and Q. Zeng, *Chin. Chem. Lett.*, 2020, **31**, 10–18.
22 J. F. Dienstmaier, K. Mahata, H. Walch, W. M. Heckl, M. Schmittel and M. Lackinger, *Langmuir*, 2010, **26**, 10708–10716.
23 O. Ochs, M. Hocke, S. Spitzer, W. M. Heckl, N. Martsinovich and M. Lackinger, *Chem. Mater.*, 2020, **32**, 5057–5065.
24 A. Badami-Behjat, P. S. Deimel, F. Allegretti, E. Ringel, K. Mahata, M. Schmittel, J. V. Barth, W. M. Heckl and M. Lackinger, *Chem. Mater.*, 2022, **34**, 8876–8884.
25 L. Kampschulte, M. Lackinger, A.-K. Maier, R. S. K. Kishore, S. Griessl, M. Schmittel and W. M. Heckl, *J. Phys. Chem. B*, 2006, **110**, 10829–10836.
26 R. Gutzler, S. Lappe, K. Mahata, M. Schmittel, W. M. Heckl and M. Lackinger, *Chem. Commun.*, 2009, 680–682.
27 J. Li, B. Tu, X. Li, C. Ma, C. Chen, W. Duan, X. Xiao and Q. Zeng, *Chem. Commun.*, 2019, **55**, 11599–11602.
28 H. Dai, S. Wang, I. Hisaki, S. Nakagawa, N. Ikenaka, K. Deng, X. Xiao and Q. Zeng, *Chem.–Asian J.*, 2017, **12**, 2558–2564.
29 Y. Zhang, P. Lei, T. Meng, K. Deng, X. Xiao and Q. Zeng, *New J. Chem.*, 2023, **47**, 7716–7721.
30 L. Y. Zhang, J. L. Li, S. H. Qiu, X. B. Huang and Z. B. Zeng, *New J. Chem.*, 2017, **41**, 3260–3264.
31 J. M. MacLeod, O. Ivasenko, C. Y. Fu, T. Taerum, F. Rosei and D. F. Perepichka, *J. Am. Chem. Soc.*, 2009, **131**, 16844–16850.
32 Z. Ma, Y.-Y. Wang, P. Wang, W. Huang, Y.-B. Li, S.-B. Lei, Y.-L. Yang, X.-L. Fan and C. Wang, *ACS Nano*, 2007, **1**, 160–167.
33 S. L. Lee, Y. Fang, G. Velpula, F. P. Cometto, M. Lingenfelder, K. Müllen, K. S. Mali and S. De Feyter, *ACS Nano*, 2015, **9**, 11608–11617.

34 R. Gutzler, T. Sirtl, J. F. Dienstmaier, K. Mahata, W. M. Heckl, M. Schmittel and M. Lackinger, *J. Am. Chem. Soc.*, 2010, **132**, 5084–5090.
35 F. P. Cometto, K. Kern and M. Lingenfelder, *ACS Nano*, 2015, **9**, 5544–5550.
36 S. Y. Li, X. Q. Yang, T. Chen, D. Wang, S. F. Wang and L. J. Wan, *ACS Nano*, 2019, **13**, 6751–6759.
37 X. Zeng, S. B. Khan, A. Mahmood and S. L. Lee, *Nanoscale*, 2020, **12**, 15072–15080.
38 A. Mahmood, X. Zeng, A. S. Saleemi, K. Y. Cheng and S. L. Lee, *Chem. Commun.*, 2020, **56**, 8790–8793.
39 C. Deng, Z. Liu, C. Ma, H. Zhang and L. Chi, *Langmuir*, 2020, **36**, 5510–5516.
40 M. Saeed, A. Mahmood, A. S. Saleemi, X. Zeng and S. L. Lee, *J. Phys. Chem. C*, 2020, **124**, 829–835.
41 A. Mahmood, M. Saeed, Y. Chan, A. S. Saleemi, J. Guo and S.-L. Lee, *Langmuir*, 2019, **35**, 8031–8037.
42 C. N. Morrison, S. Ahn, J. K. Schnobrich and A. J. Matzger, *Langmuir*, 2011, **27**, 936–942.
43 F. Hu, Y. Gong, X. Zhang, J. Xue, B. Liu, T. Lu, K. Deng, W. Duan, Q. Zeng and C. Wang, *Nanoscale*, 2014, **6**, 4243–4249.
44 S. Zhang, J. Zhang, K. Deng, J. Xie, W. Duan and Q. Zeng, *Phys. Chem. Chem. Phys.*, 2015, **17**, 24462–24467.
45 J. A. Elemans, I. De Cat, H. Xu and S. De Feyter, *Chem. Soc. Rev.*, 2009, **38**, 722–736.
46 K.-H. Ernst, *Phys. Status Solidi B*, 2012, **249**, 2057–2088.
47 R. Raval, *Chem. Soc. Rev.*, 2009, **38**, 707–721.
48 T. Chen, D. Wang and L.-J. Wan, *Natl. Sci. Rev.*, 2015, **2**, 205–216.
49 K. E. Plass, A. L. Grzesiak and A. J. Matzger, *Acc. Chem. Res.*, 2007, **40**, 287–293.
50 S. Dutta and A. J. Gellman, *Chem. Soc. Rev.*, 2017, **46**, 7787–7839.
51 Y. Xu, J.-J. Duan, Z.-Y. Yi, K.-X. Zhang, T. Chen and D. Wang, *Surf. Sci. Rep.*, 2021, **76**, 100531.
52 I. Hisaki, Y. Sakamoto, H. Shigemitsu, N. Tohnai, M. Miyata, S. Seki, A. Saeki and S. Tagawa, *Chem.–Eur. J.*, 2008, **14**, 4178–4187.
53 J. Y. Choi, J. Kim, H. Furukawa and H. K. Chae, *Chem. Lett.*, 2006, **35**, 1054–1055.
54 R. Lazzaroni, A. Calderone, G. Lambin, J. P. Rabe and J. L. Brédas, *Synth. Met.*, 1991, **41**, 525–528.
55 H. S. Lee, S. Iyengar and I. H. Musselman, *Langmuir*, 1998, **14**, 7475–7483.
56 T. Steiner and G. R. Desiraju, *Chem. Commun.*, 1998, **8**, 891–892.
57 T. Steiner, *Angew. Chem., Int. Ed.*, 2002, **41**, 48–76.
58 G. R. Desiraju, *Acc. Chem. Res.*, 1996, **29**, 441–449.
59 G. Eder, S. Kloft, N. Martsinovich, K. Mahata, M. Schmittel, W. M. Heckl and M. Lackinger, *Langmuir*, 2011, **27**, 13563–13571.
60 S. J. H. Griessl, M. Lackinger, F. Jamitzky, T. Markert, M. Hietschold and W. M. Heckl, *Langmuir*, 2004, **20**, 9403–9407.